PFC/JA–89–46

Submillimeter Wave Harmonic Gyrotron Experiment

Spira–Hakkarainen, S., Kreischer, K.E., Temkin, R.J.

Plasma Fusion Center

Massachusetts Institute of Technology

Cambridge, MA 02139

September 1989

This work was supported by U.S. DOE Contract DE–AC02–78ET51013.

SUBMILLIMETER WAVE HARMONIC GYROTRON EXPERIMENT

S. Spira-Hakkarainen, K. E. Kreischer, R. J. Temkin

ABSTRACT

This paper reports a theoretical and experimental investigation of the operation at submillimeter wavelengths of a harmonic gyrotron. Using a waveguide cavity with an iris at the output end of the straight section, fourteen different second harmonic modes were observed with frequencies between 301 - 503 GHz, output powers of 1 - 22 kW, and a 12 MHz emission frequency bandwidth. The highest output power was 22 kW with a total efficiency of 3.5% at 467 GHz, and an output power of 15 kW with a 6% efficiency was obtained at 417 GHz. Research was conducted using a 65 - 75 kV, up to 10 A electron gun with 1 - 1.5 μsec pulselength and a 4 Hz repetition rate, that produced a helical electron beam in magnetic fields of up to 14 Tesla. These results represent the first operation of a high power harmonic gyrotron in the submillimeter region.

INTRODUCTION

High power submillimeter microwave sources have many potential applications. In plasma applications, these sources can be used for electron cyclotron resonance heating[1] and plasma diagnostics[2]. High frequency devices are also important for applications such as a space based radar system, communications systems and material science[2,3] applications which require a stable, narrow linewidth source.

Very few devices operate in the submillimeter regime. Gyrotrons fill a gap between conventional microwave devices (magnetrons, klystrons, triodes, etc.) and lasers. Although far infrared lasers operate in this regime, efficiencies are less than 0.1 %[4]. Gyrotrons have advantages over other devices that operate in this regime. Free electron lasers (FEL) [5,6,7,8] and cyclotron resonance masers [9,10,11,12] (CARM) are large devices that require high voltage (> 500 kV) power supplies. Since gyrotrons are weakly relativistic devices, lower voltage (60 - 100 kV) supplies can be used. Cherenkov sources [13,14,15] also operate in this frequency range, but are higher in voltage and lower in efficiency than gyrotrons.

The primary goal of this experiment is to achieve high power, submillimeter emission. To attain frequencies in the submillimeter region using fundamental mode operation, magnetic fields above 12 T would be required. The advantage gained by using harmonic operation is that lower magnetic fields are needed for second harmonic than fundamental interactions. To operate at 300 GHz, using a second harmonic mode requires just a 6 T field available from a conventional NbTi superconducting magnet, instead of 12 T required for a fundamental interaction.

Past second harmonic results show that second harmonic emission is experimentally possible at high frequency and powers. In the Soviet Union, at 154 GHz, 7 kW was produced with pulsed operation and with cw operation, 2.4 kW at 157 GHz and 1.5 kW at 326 GHz were observed [16]. At M.I.T., Byerly et al. [17] observed stable second harmonic emission from 209 GHz to 302 GHz, with a peak power of 25 kW at 241 GHz, in 1 μs pulsed operation.

When conducting a second harmonic experiment the basic physics issues must be studied in order to understand how to optimize the design of a second harmonic gyrotron. A major issue is mode competition, both between fundamental and second harmonic modes as well as between two or more harmonic modes. The mode competition between the fundamental and harmonic modes, however, is the dominant issue. Second harmonic modes are difficult to excite for several reasons. Firstly, their starting currents are often higher

than those of adjacent fundamental modes. As a result, the fundamental modes get excited first, and then suppress the second harmonic modes. Secondly, the highly overmoded cavities used to reduce ohmic losses also make mode competition more severe. Mode density increases as the cavity size becomes larger, thereby making mode competition more severe. Finally, the relatively thick beam produced by our gun further aggravates the mode competition problem, because the beam can couple to several modes simultaneously.

An earlier experiment was conducted at MIT with a tapered cavity similar to the cavities described in this paper, except it had no iris. When this experiment was conducted, only low frequency (< 300 GHz) harmonics were observed. At higher frequencies, the fundamental spectrum was very dense and the harmonic modes were suppressed.

In this paper, the design and experimental results of a harmonic gyrotron experiment are presented. Fourteen second harmonic modes were observed in the frequency range of 301 GHz to 503 GHz, with power levels of 1 - 22 kW. The organization of this paper is as follows. Section 2 outlines the basic gyrotron theory. The experimental setup used to conduct the experiments described in this paper, the techniques of fundamental mode suppression used and other resonator design considerations are contained in Section 3. Next, in Section 4 the experimental results are discussed. This includes a comparison of the theoretical efficiency and gain and the experimental values. The conclusions are presented in Section 5.

2 Theory

The gyrotron discussed in this paper has a weakly tapered cylindrical resonator, so the TE_{mpq} modes of a circular cylindrical cavity can be used to represent the modes excited in this device. The subscripts m, p, and q are the azimuthal, radial and axial mode indices respectively. The oscillation frequency of a TE_{mpq} mode is

$$\omega^2/c^2 = k^2 = k_\perp^2 + k_\parallel^2 \tag{1}$$

where $k_\perp = \nu_{mp}/R_o$, $k_\parallel = 2q/L_{eff}$ for a Gaussian axial RF field profile in the cavity, R_o and L_{eff} are the cavity radius and effective interaction length, respectively, and ν_{mp} is the p^{th} root of $J'_m(x) = 0$.

In a gyrotron, an electron beam loses energy to an RF wave by passing through a resonator near cutoff ($k_\perp \gg k_\parallel$). The frequency ω of the emitted coherent radiation is approximately given by the excitation condition of the gyrotron instability

$$\omega - k_{||}\beta_{||}c = n\omega_c \tag{2}$$

with the cyclotron frequency $\omega_c = eB_o/\gamma m$, $\gamma^{-2} = (1-\beta^2)$, the total normalized beam velocity $\beta = v/c$, $\beta_\perp$, $\beta_{||}$ are the perpendicular and parallel components of the normalized velocity with respect to the direction of the main field B_o and n is the harmonic number. Since $k_\perp \gg k_{||}$ we also have $\omega \simeq c\nu_{mp}/R_o \simeq n\omega_c$. When the magnetic field is varied it is possible to excite a sequence of discrete modes with different ν_{mp}, and different frequencies, ω.

A mode of frequency ω can only oscillate over a small region in B_o. To determine the region of excitation for a mode, the linearized equations of motion [18] and the equilibrium condition in the cavity, which defines the cavity Q (Q = power stored per cycle/power dissipated per cycle), must be used. By combining these equations, one can derive a threshold condition for the electron beam current required for oscillation of a mode given by

$$I_{st} = \frac{4}{\pi\mu^2}\frac{e^{2x^2}}{\mu x - n} \tag{3}$$

where I_{st} is the starting current normalized as in Eq. (4) below, $\mu = (\pi\beta_{\perp o}^2/\beta_{||o})(L_{eff}/\lambda)$ is a normalized interaction length, λ is the wavelength, $x = \mu\Delta/4$, $\Delta = 2(1-n\omega_{co}/\omega)/\beta_{\perp o}^2$ and the subscript o refers to quantities at the entrance of the resonator. The minimum starting current, $I_{st\ min}$, occurs at $x = x_{min} = (1/2)(n/\mu + \sqrt{n^2/\mu^2+1})$. The expression required to convert the normalized beam current, I, to amperes is given by

$$I = 0.239\times 10^{-3}\frac{Q_T I_a}{\gamma_o}\beta_\perp^{2(n-3)}\left(\frac{\lambda}{L}\right)\left(\frac{n^n}{2^n n!}\right)^2\frac{J_{m\pm n}^2(k_\perp R_e)}{(\nu_{mp}^2-m^2)J_m^2(\nu_{mp})} \tag{4}$$

where the total Q, Q_T, incorporates the diffractive (Q_D) and ohmic losses (Q_{oh}) and $Q_T^{-1} = Q_D^{-1} + Q_{oh}^{-1}$, I_a is the beam current in amperes, and R_e is the radial position of the electron beam.

3 Experimental Design

A schematic of the system is shown in Figure 1, which is discussed in more detail by Temkin et al[19]. On the far left side is the electron gun, which produces an annular electron beam. In the experiments described in this paper the electron beam was generated by a Varian pulsed magnetron injection gun [20], with a peak current of 10 A at 73 kV and a pulselength of 1 - 2 μsec at a 4 Hz repetition rate. A copper, water cooled Bitter magnet is used to produce the dc magnetic field. The beam moves to the right into a region of magnetic compression. After leaving the resonator, which is in a constant high magnetic field, the beam follows the magnetic field lines which cause it to be deposited on a copper

collector. The collector also acts as an overmoded waveguide for the radiation generated by the resonator and the microwaves leave the vacuum region by passing through a fused quartz window.

To suppress the fundamental modes, an electromagnetic structure was designed where the Q of the second harmonic modes was increased significantly and the Q of the fundamental modes was fairly unchanged. To accomplish this, a small iris was placed at the output end of the cavity straight section. The effect of the iris is to trap the second harmonic modes more effectively than the fundamental modes. Since gyrotrons operate near cutoff, an iris with a small reduction in radius ($\leq$ 0.01 in) will extend below the cutoff radius. Extending an iris below the cutoff radius creates a region where the RF field is an evanescent wave. The iris region can be made evanescent for the second harmonic modes while not being evanescent (cutoff) for the fundamental modes. This allows the cavity Q of the second harmonic modes to be increased relative to that of the fundamental modes, thus helping to discriminate in favor of second harmonic operation of the gyrotron.

The relative values of the Q of the fundamental and second harmonic modes can be demonstrated by the following illustrative example. This example indicates the design philosophy; detailed designs were carried out using a numerical analysis which solves for the cavity eigenmodes of realistic configurations. Consider the simplified cavity illustrated in Figure 2. Modes are generated in the circular cylinder cavity region of radius R_c and length L_c and are coupled out of the cavity through an iris region of radius R_i and length L_i. A second harmonic mode of frequency ω_2 generated in the cavity satisfies the cavity resonance condition:

$$\frac{\omega_2^2}{c^2} = \frac{\nu_2^2}{R_c^2} + \left(\frac{\pi}{L_c}\right)^2 \tag{5}$$

$$\omega_2 \approx 2\omega_c$$

where a right circular cylinder cavity is assumed and ν_2 is the appropriate Bessel function root for the second harmonic mode. In the iris region the axial wavenumber of the mode, as it propagates away from the cavity, is given by:

$$k_{\|,2}^2 = \frac{\omega_2^2}{c^2} - \frac{\nu_2^2}{R_i^2} \tag{6}$$

For this example, we may choose the iris radius, R_i, so that the mode of frequency ω_2 is exactly cutoff in the iris region, that is

$$k_{\|,2} = 0$$

Now consider a mode at the fundamental frequency ω_1 generated in the same cavity at the same, or nearly the same, magnetic field:

$$\frac{\omega_1^2}{c^2} = \frac{\nu_1^2}{R_c^2} + \left(\frac{\pi}{L_c}\right)^2 \tag{7}$$

$$\omega_1 \approx \omega_c$$

The axial wavenumber of this mode, in the iris region, is given by:

$$k_{\|,1}^2 = \frac{\omega_1^2}{c^2} - \frac{\nu_1^2}{R_i^2} = \frac{\nu_1^2}{R_c^2} - \frac{\nu_1^2}{R_i^2} + \left(\frac{\pi}{L_c}\right)^2 \tag{8}$$

Using Equations (5) and (6), we have

$$\frac{\nu_2^2}{R_c^2} - \frac{\nu_2^2}{R_i^2} + \left(\frac{\pi}{L_c}\right)^2 = 0 \tag{9}$$

Substituting this result in Equation (8), we have

$$k_{\|,1}^2 = \left(\frac{\pi}{L_c}\right)^2 \left(1 - \frac{\nu_1^2}{\nu_2^2}\right) \tag{10}$$

But, $\omega_1/\omega_2 \approx 1/2$ and since $k_\perp \gg k_\|$ in the cavity, $\nu_1/\nu_2 \approx 1/2$. This yields the result

$$k_{\|,1} \approx \frac{\sqrt{3}}{2}\left(\frac{\pi}{L_c}\right) \tag{11}$$

This illustrative example indicates the basic design features of the gyrotron iris cavity. If the iris is just sufficient to cutoff the second harmonic mode, as is the case in this example, Equation (11) indicates that the fundamental mode can still propagate through the iris region. In fact, the axial wavenumber of the fundamental mode in the iris region is only slightly lower than in the cavity itself, reduced by only $\sqrt{3}/2$.

These results prove that an iris can have a dramatic result on the confinement (or Q) of a second harmonic mode while only very weakly affecting modes at the fundamental.

As the length of the iris region, L_i, is extended, the second harmonic mode diffractive Q increases dramatically while the Q of the fundamental mode grows slowly. This shows that the ratio of the Q values at the two frequencies can, in principle, be made arbitrarily large. This is a remarkable result. The iris cavity, in principle, can provide complete mode discrimination between modes at the fundamental and second harmonic in favor of the higher frequency mode.

In practice, the mode discrimination effect is limited. First, the diffractive Q cannot be made arbitrarily large since it should not exceed the ohmic Q. Second, the cavities are not closed at the ends, as in the right circular cylinder, but have large openings. The axial wavenumber, $k_{\|}$, in the cavity is not given by π/L but by $2/L_{eff}$, where L_{eff}, the effective cavity length, has some mode dependence. Nevertheless, the general features of the iris cavity described above are verified by numerical analysis of actual gyrotron cavity designs.

A study was conducted to determine the effect of iris shape on the fundamental to second harmonic starting current (in Amperes) ratio, I_{ast1}/I_{ast2} and to optimize the cavity design for a given diffractive Q of the second harmonic mode. The ratio I_{ast1}/I_{ast2} is a measure of how strong the second harmonic can become before the fundamental mode is excited. If this ratio exceeds unity, linear theory predicts that there are operating regimes in which second harmonic modes can be excited without competition from fundamental modes. A simplified expression can be obtained for this ratio by combining equations (3) and (4) and assuming that $\mu \gg n$, $\nu_{mp}^2 \gg m^2$, $\nu_{mp} \propto k = 2\pi/\lambda$, and $\lambda_2 \simeq \lambda_1/2$ where the subscripts 1 and 2 refer to fundamental and second harmonic quantities. Since whispering gallery modes are the most easily excited second harmonic modes it can be also assumed that $m \gg 1$ and p is small, and $J_{m\pm n}(k_\perp R_e) \simeq J_m(\nu_{mp})$ if the beam is positioned on the innermost peak of the coupling term $J_{m\pm n}(k_\perp R_e)$. Using these approximations, we find that the starting current ratio is given by:

$$I_{ast1}/I_{ast2} \simeq \beta_\perp^2 \left(\frac{L_{eff2}}{L_{eff1}}\right)^2 \left(\frac{Q_{T2}}{Q_{T1}}\right) \tag{12}$$

where $\beta_\perp$ is a constant for this study, since it is unaffected by the cavity geometry.

The ratio in Equation (12) was studied for two modes of interest, the second harmonic design mode, $TE_{13,2,1}$ and the strongest neighboring fundamental mode, the $TE_{5,2,1}$. The ratio of the fundamental to second harmonic L_{eff} does not vary significantly when the iris dimensions are changed. The diffractive Q, however, is strongly affected by the iris dimensions. As the iris becomes a bigger potential barrier, by becoming thicker, deeper or

having shallower inner or outer angles, the reflection coefficient of waves from the cavity incident on the iris increases. L_{eff} decreases, but that effect is small. For any given iris size and therefore second harmonic diffractive Q (for a fixed cavity length), we obtain an almost constant value of the fundamental Q_D. The diffractive Q ratio, Q_{D2}/Q_{D1}, increases as the iris size is increased, so therefore one would like to operate with as high a second harmonic diffractive Q as possible. However, since $I_{ast} \propto 1/Q_T$, at high diffractive Q the total Q ratio saturates due to the effect of the ohmic Q. This leads to a saturation in I_{ast} as a function of Q_D, when the value of the diffractive Q begins to approach that of the ohmic Q. As a result, it is not desirable to operate with a second harmonic diffractive Q whose value approaches that of the ohmic Q of that mode.

The saturation value of the total Q ratio, Q_{T2}/Q_{T1}, can be increased by using a mode with a higher ohmic Q. As the radial index, p, (TE_{mpq} modes) is increased, higher ohmic Q values for a given cavity radius result. However one must consider the effect on the starting current of operating with a higher p mode. The starting current is influenced by the coupling coefficient of the mode, $J^2_{m\pm n}(k_\perp R_e)/J^2_m(\nu_{mp})(\nu^2_{mp} - m^2)$. When considered as a function of beam radius it is found that the optimal coupling coefficient occurs on the innermost radial maximum of the mode. Since the beam position determines the maximum value of m, modes with higher p values can be accessed by operating with a larger cavity radius. However as the cavity radius is increased, mode density increases and mode competition problems become worse, due to the higher mode density. Therefore modes with $p > 3$ were not considered. The benefit of operating with a higher p index is illustrated by the fact that the modes where p = 3 are the high power modes, as will seen in the experimental data section.

The decision to use an existing electron gun imposed a number of constraints on the system. The cathode radius of the gun is 0.92 cm and past experience has shown that a magnetic field at the cathode of 0.23 Tesla is needed for high efficiency operation[22]. Therefore, the existing gun has a beam radius R_e, $k_\perp R_e \simeq 13.0$, for operation at 400 GHz with a main field around 8 Tesla. The other system constraints are a maximum beam current of 10 Amps at a cathode voltage of 65 kV with a pulselength of 1 - 2 μsec and $\beta_\perp/\beta_{||} = 1.5$.

Two main criteria were used to select the design mode, strong beam-RF interaction and weak surrounding fundamental modes. The $TE_{13,2,1}$ mode satisfied the criterion of weak surrounding fundamental modes and the beam could be placed at the innermost (and biggest) maximum of the coupling coefficient which corresponded to a beam position, $k_\perp R_e$, of 12.8. Selecting a mode specifies the cavity radius. Next the cavity length and

iris dimensions must be chosen. The determination of iris dimensions and cavity length is governed by the tradeoff between a high starting current ratio, I_{ast1}/I_{ast2} and high perpendicular and ohmic efficiencies. In this experiment, to ensure that the fundamental mode was not excited too easily, the theoretical starting current of the strongest fundamental mode was required to be above 1 A. The tapers are designed to maximize fundamental mode leakage, but also the tapers must have shallow angles ($\leq 5°$) to minimize mode conversion problems.

Table 1 lists the design parameters for a 100 kW, 410 GHz second harmonic gyrotron operating in the $TE_{13,2,1}$ mode. The resonator was designed to produce 100 kW to demonstrate high power operation. The iris was constrained in two ways. The first constraint was that the minimum iris depth was 0.005 cm, which was the smallest depth that could be reliably machined. A 0.005 cm iris was the deepest iris that would not produce a fundamental starting current that was too low and create severe ohmic losses due to a second harmonic diffractive Q that was too high. To minimize the diffractive Q, the output taper angle was chosen to be as large as possible without causing significant mode competition problems. The value chosen was 5°. The straight section length was shortened to a length of 0.526 cm, which was the minimum length that theoretically produced 100 kW at 65 kV and 9 Amps. The design current was chosen to be 9 A, since this is the highest current that the gun can be expected to reliably produce. As a result of the second harmonic diffractive Q being very high, the ohmic efficiency defined as $Q_{OH}/(Q_D + Q_{OH})$ has now been reduced to 56.4%. The magnetic field of 8.3 T corresponds to the minimum starting current. In Figure 3 we show a schematic of the resonator's actual dimensions and the RF field profiles of the $TE_{13,2,1}$ and the $TE_{5,2,1}$, modes. In the diagram it can be seen that the second harmonic mode is more trapped than the fundamental mode.

Figures 4 a and b show the effect of the iris on second harmonic and fundamental starting currents [23] where no beam spread effects were assumed. The $TE_{4,2,1}$ and the $TE_{5,2,1}$ are the strongest fundamental modes near the design mode for this resonator radius. Two cases of starting current as a function of magnetic field were calculated, the case using the actual cavity dimensions (iris case) and a "no iris" case. In the latter case, the iris was flattened creating a slightly longer flat section. The presence of the iris decreases the starting current ratio, I_{st1}/I_{st2} by a factor of 1.8 to become unity. This indicates that the iris represents a significant improvement, but that the improvement is limited. In the present experiments, that limit is directly the result of the relatively low ohmic Q that is found in high frequency experiments. Far better results might be obtained at lower frequency where ohmic loss is less important.

4 Experimental Results

Initially the experiment was run with a cathode voltage of 65 kV. However, when the voltage was increased to 73 kV the harmonic modes became stronger. This can be understood as follows. As the cathode voltage increases, the perpendicular velocity, $\beta_\perp$ increases. A larger $\beta_\perp$, results in higher efficiency and a larger fundamental to second harmonic starting current ratio (see equation 12). The second harmonic modes also became stronger when the mod anode voltage was decreased. This may be a result of the fact that in practice the gun is nonadiabatic and tends to be very sensitive to mod anode voltage. Since the gun was being run at a higher cathode voltage than it was designed for, lower mode anode voltages may correspond to better beam quality or higher α ($= \beta_\perp/\beta_\parallel$).

Experimentally, twelve second harmonic modes ranging from 301 to 503 GHz were observed and these modes are listed in Table 2. The power, frequency, and efficiency are given for each of the second harmonic emissions, as well as the theoretical mode that most closely corresponds to the frequency. The power measurements were all taken at a cathode voltage of 73 kV. In the measurements at 417 GHz and 467 GHz, the emission was found to be purely second harmonic emission, with no significant fundamental present at the same time. Evidence for this is obtained from video diode and calorimeter measurements. Emission at the fundamental and harmonic frequencies could be differentiated by using a waveguide cutoff filter or combined horn and filter in front of the video detector. Quantitative information on the fraction of power at the two frequencies could be obtained using a calorimeter with plexiglass sheets of varying thickness. The transmission of the plexiglass sheets varies strongly with frequency and was independently calibrated using fixed frequency sources. The emission frequency was measured using a harmonic mixer system[24]. Strong signals were observed in a diode with a filter horn that transmits frequencies above 400 GHz. At 417 GHz, 15 kW of power was measured, which corresponds to a 6% total efficiency. The other modes ranging from 301 GHz to 503 GHz had powers of 3-14.2 kW and efficiencies of 0.6%-5.73%. Measurements with higher current were not possible, because when the beam current increased the fundamental modes get excited and suppress the second harmonic modes.

At low frequencies several second harmonic p=1 modes are present, but disappear at higher frequency (higher magnetic fields) as the beam moves away from the cavity wall with increasing compression caused by the higher magnetic fields. As noted previously, the p=3 modes are the highest efficiency modes and, in particular, the $TE_{10,3,1}$ and the $TE_{11,3,1}$ were the highest power modes in this experiment.

Figure 5 shows the regions of excitation for a fixed cathode voltage of 73 kV, 22.9

kV mod anode voltage, and 3 ampere beam current as a function of magnetic field at the cavity and magnetic field at the cathode. Varying the cathode magnetic field corresponds to changing the ratio of perpendicular to parallel velocity, $v_\perp/v_{||}$, which changes the starting current of a given mode. As magnetic field at the gun is decreased, perpendicular velocity increases. The graph in Figure 5 was generated by fixing the main field and continuously varying the field at the gun. The process was repeated for a number of discrete values of the main field. The boundaries of each mode are determined by whether the corresponding frequency is observed by the frequency system. This is done because using just the video diode signal can lead to inaccuracies when more than one fundamental mode is being excited. Each of the regions of second harmonic emission in Figure 5 corresponds to regions where that second harmonic mode was observed, including areas with a second harmonic and fundamental mixture. In this mode map , the step tunable behavior of the second harmonic emission, similar to that described by Kreischer[25] for the fundamental emission, can be seen. When the harmonic mode is not being suppressed by a strong fundamental mode, the p = 1,2,3 ($TE_{m,p,q}$) sequences are excited, with m values in the range of 8 to 17. The region of excitation for the $TE_{17,2,1}$ was found to be smaller than the other second harmonic modes, and above a main field of 10.2 T no second harmonic modes were observed. At higher fields, the fundamental and second harmonic spectra become sparser, since beam compression is increased and therefore the beam quality is diminished. Poorer beam quality (larger pitch angle spread) and a decrease in the ratio $\beta_\perp/\beta_{||}$, result in less of the beam energy coupling to the RF-wave. These effects raise the starting currents and decrease the starting current ratio, which scales as $I_{st1}/I_{st2} \propto \beta_\perp^2$.

5 Experimental Results with a Motheye Window

In this section, another method of reinforcement that was used to supplement the iris's effect will be described. Using a motheye window [26] instead of an ordinary quartz window proved to be very effective, and required only the window mount to be slightly enlarged. A motheye window is fabricated by cutting two perpendicular sets of sawtooth grooves which form pyramidal protuberances on both of the window's surfaces. These protuberances act as a gradation for the refractive index and thereby reduce window reflections for a broad band of frequencies as shown in Figure 6. The window used in this experiment had a transmission coefficient of 0.8 or greater from 100-300 GHz. From 300-400 GHz the transmission coefficient drops to 0.2 and varies from 0 to 0.2 at higher frequencies. This reduced transmission is mainly due to increased reflection rather than absorption. The transmission coefficient measurement was made with a broadband source and a spectrometer [27]. Since the reflection characteristics of the window are high at high frequency, and low at low frequency, only the diffractive Q of the second harmonic is significantly increased.

The effect of the motheye window can be seen in the mode map shown in Figure 7, where the regions of second harmonic excitation are bigger than those in the mode map shown in Figure 5, which corresponds to a regular quartz window. It is also noticed that the $TE_{13,2,1}$ and $TE_{9,3,1}$ modes were present in this case but not in Figure 5. The regions of second harmonic emission are larger at frequencies above 390 GHz where the motheye window reflects, than the regions of the second harmonic modes with frequencies less than 390 GHz, such as the $TE_{16,1,1}$, the $TE_{8,3,1}$, or the $TE_{11,2,1}$. This is consistent with the measurement of the reflector and transmission coefficient as a function of frequency, with the result that the transition region between good and poor transmission is somewhere between 300 and 400 GHz. As mentioned earlier, operation at higher values of the main magnetic field may cause beam degradation. For second harmonic modes, this is somewhat counterbalanced by the increase of Q_D due to the motheye window.

In Table 3 the power, frequency, efficiency and theoretical mode are listed for the observed modes. All of those modes above 339 GHz that were also observed using a quartz window are in that list, except for the $TE_{11,3,1}$ mode, as well as the new modes, the $TE_{9,3,1}$ and the $TE_{13,2,1}$. The $TE_{11,3,1}$ may correspond to a different tube alignment, and therefore was not observed when the motheye window was used. The $TE_{12,3,1}$ and the $TE_{17,2,1}$ modes are stronger when the motheye window is used. The presence of the $TE_{9,3,1}$ and the $TE_{13,2,1}$ modes as well as the higher power levels observed for the $TE_{17,2,1}$ and the $TE_{12,3,1}$ modes indicate that the motheye window is reinforcing the higher frequency ($>$ 390 GHz) modes. The lower power level of the $TE_{10,3,1}$ mode may have been due to poor alignments with a non-optimal beam position. This can be postulated because in the mode map shown in Figure 7 the region of excitation is larger than when using the quartz window. With more modes present, the step tunable behavior is more pronounced, with an average step size of 10 GHz between modes. If different alignments had been explored, it is quite likely that the $TE_{12,2,1}$, $TE_{14,2,1}$ and the $TE_{16,2,1}$ modes would also have been observed. All of the modes from m=8 to m=13 were observed in the p=3 family of modes, supporting the theory that the p=3 modes are more efficient and have lower starting currents than the p=2 modes.

A comparison between the experimental and theoretical efficiency was also made for both windows. The peak power and efficiency of the $TE_{12,3,1}$ second harmonic mode measured as a function of beam current at a fixed cathode voltage was analysed. Figure 8a shows the theoretical efficiency as a function of beam current with the cathode voltage at 73.1 kV (all the power measurements were at this voltage) and $\alpha = v_\perp/v_\parallel = 1.5$. The open circles denote the case with no correction calculated from the nonlinear theory [18]. So far we have assumed that the only losses are the power diffracting out of the cavity and

the ohmic losses in the straight section. However losses also occur in the output taper of the resonator, the collector and in the window. From Figure 6, where the dashed line is the transmission characteristic of a plain quartz window, we can see that at this frequency 60% of the power will be transmitted through the window. The formula used to calculate the ohmic losses in the uptaper and the collector is given in Collin [28]. The collector has a fixed radius of 1.1 cm and it is 61 cm long. These parameters give the collector a 97.4% efficiency. The linear, 5° output taper starts at a radius of 0.2265 cm and ends up at a radius of 1.1 cm over a distance of 14.9 cm and the uptaper efficiency is 98.1%. The filled circles represent the results including all of these effects and give the theoretical predictions to which the experimental results are compared.

When a quartz window was used, the power saturated at 7 kW with a peak efficiency of 4.9% and a beam current of 2 amperes, as shown in Figure 8b. With the beam current above 3 amperes it was not possible to find an operating point where the fundamental mode was absent. It is seen that the peak efficiency is higher than predicted by theory. The reason may be the ratio of perpendicular velocity to parallel velocity may be higher than the value of 1.5.

With the motheye window, Figure 8c, it was possible to observe single mode emission at currents up to 9 amperes and therefore generate higher output power. The highest observed power was 17.8 kW with an efficiency of 2.8% at a beam current of 7.8 amperes. This suggests that the motheye window significantly reinforces only the second harmonic modes. The discrepancy between the theoretical and experimental efficiencies may be explained in part by the fact that the data in Figure 8c were only taken at operating points where no fundamental was observed. Therefore the detuning and value of α in the operating points where the experimental data were taken may not have been as optimal as the values used for the theoretical calculation.

6 CONCLUSIONS

Submillimeter second harmonic emission was successfully excited. In order to excite these modes, fundamental mode suppression techniques were required, such as using an iris. When a cavity with an iris at the output end of the straight section was used with an ordinary quartz window, twelve different second harmonic modes were observed with frequencies ranging from 301 to 503 GHz. At 417 GHz, 15 kW of power was measured, which corresponds to a 6% total efficiency. The other second harmonic modes had power levels of 3 - 14.6 kW and efficiencies of 0.6 - 5.7%. The iris cavity was found to significantly enhance the excitation of second harmonic modes. In a preliminary experiment, a cavity

was tested which was similar to the iris cavity but had no iris. That cavity did not oscillate at any second harmonic frequencies when operated at higher magnetic fields. The good results with the iris cavity demonstrate conclusively the advantages of an iris cavity for high frequency, harmonic operation. When a motheye window was used (with the same cavity) to provide external feedback to the second harmonic mode, two new second harmonic modes were observed. At 467 GHz, 22 kW of power was measured with a 3.4% total efficiency, and the other modes had power levels of 1 - 10 kW and total efficiencies of 0.7 - 5.3%. The bandwidth of these second harmonic modes was measured on a single shot basis using the harmonic mixer system. Typical bandwidths were about 12 GHz which is relatively narrow. The bandwidths may have been less than 12 MHz, however the mixer sensitivity limit is 12 MHz. The effect of the motheye window was to slightly increase the region of excitation and slightly lower the starting current of the second harmonic modes, thereby allowing two extra second harmonic modes to be excited. The reflected power from the motheye window would be unattractive for high average power operation. However, for pulsed operation at moderate average power it appears to be very useful. In these two iris cavity experiments, step tunable behavior for the second harmonic modes was observed. When the harmonic modes were not being suppressed by the fundamental modes, the p = 1,2,3 ($TE_{m,p,q}$) sequences were excited.

ACKNOWLEDGMENTS

This work was supported by the U.S. Department of Energy under Contract No. DE–AC02–78ET51013. The Bitter magnet was provided by the National Magnet Laboratory under the support of the National Science Foundation. The authors wish to thank W. Mulligan, C.Y. Wang, P. Lentini, S. Chu, M. Afsar, and T. Kozul for valuable discussions and assistance.

REFERENCES

(1) R. Prater, Proc. Eighth Topical Conference on Radio Frequency Power in Plasmas, Irvine, California, (1989).

(2) P. Woskoboinikow, D.R. Cohn, M. Gerver, W.J. Mulligan, R.S. Post, R.J. Temkin and J. Trulsen, Rev. Scient. Instr. **56**, 914 (1985).

(3) P. Bhartia and I.J. Bahl, "Millimeter Wave Engineering and Applications", John Wiley and Sons, New York, (1984).

(4) T.A. De Temple, Pulsed Optically Pumped Far Infrared Lasers, in Infrared and Millimeter Waves, Vol. 1, K.J. Button, editor, Academic Press, N.Y. (1979).

(5) L.R. Elias, R.J. Hu, and G.J. Ramian, Nucl. Instr. Methods Phys. Res. A, **237**, (1985), p. 203.

(6) S.V. Benson, J.M.J. Madey, J. Schultz, M. Marc, W. Wadensweiler, G.A. Westenskow, and M. Velghe, Nucl. Instr. Methods Phys. Res. A, **250**, (1986), p. 39.

(7) T.C. Marshall, "Free Electron Lasers", Macmillan Publishing Company, New York, 1985.

(8) T.J. Orzechowski, B.R. Anderson, J.C. Clark, W.M. Fawley, A.C. Paul, D. Prosnitz, E.T. Scharlemann, and S.M. Yarema, Phys. Rev. Lett., **58**, (1986) p. 2172.

(9) I.E. Botvinnik, V.L. Bratman, A.B. Volkov, G.G. Denisov, B.D. Kol'chugin, M.M. Ofitserov, Pis'ma Zh. Eksp. Teor. Fiz., **8**, (1982a), p. 1376.

(10) I.E. Botvinnik, V.L. Bratman, A.B. Volkov, N.S. Ginsburg, G.G. Denisov, B.D. Kol'chugin, M.M. Ofitserov, and M.I. Petelin, Pis'ma Zh. Eksp. Teor. Fiz., **35**, (1982b), p. 418.

(11) G. Bekefi, A. Dirienzo, C. Liebovitch and B.G. Danly, Appl. Phys. Lett., **54**, No. 14, (1989), p. 1302.

(12) D.B. McDermott, H.B.Cao, and N.C. Luhmann, Jr., Conf. Dig., 13^{th} Int. Conf. on Infrared and Millimeter Waves, Honolulu, Hawaii, (1989), p. 324.

(13) E.M. Marshall, P.M. Phillips, and J.E. Walsh, IEEE 16, **2**, (1988), p. 199.

(14) A.N. Didenko, A.R. Borisov, G.R. Fomenko, and Yu.G. Shtein, Pis'ma Zh. Tekh. Fiz., **9**, (1983), p. 60.

(15) M.V. Kuzelev et al., Zh. Eksp. Teor. Fiz., **83**, (1982), p. 1358.

(16) N.I. Zaytsev, T.B. Pankratova, M.I. Petelin, and V.A. Flyagin, Radio Eng. Electron. Phys., **19**, (1974), p. 103.

(17) J.L. Byerly, B.G. Danly, K.E. Kreischer, R.J. Temkin, W.J. Mulligan, and P. Woskoboinikow, Int. J. Electron., **57**, (1984), p. 1033.

(18) B.G. Danly and R.J. Temkin, Phys. Fluids, **29**, (1986), p. 561.

(19) R.J. Temkin, K.E. Kreischer, W.J. Mulligan, S. MacCabe and H.R. Fetterman, Int. J. Inf. and MM. Waves, **3**, (1982), p. 427.

(20) K. Felch, D. Stone, H. Jory, R. Garcia, G. Wendell, R.J. Temkin, K.E. Kreischer, IEDM Tech. Dig., Paper 14.1, (1982), p. 362.

(21) A.W. Fliflet, M.E. Read, K.R. Chu and R. Seeley, Int. J. Electron **53**, 505 (1982).

(22) B.G. Danly, K.E. Kreischer, W.J. Mulligan and R.J. Temkin, Trans. Plasma Science, **PS-13**, No. 6 (1985), p. 383.

(23) K.E. Kreischer and R.J. Temkin, Infrared and MMW, Vol. 7, Chapter 8, Academic Press, N.Y. (1983).

(24) K.E. Kreischer, B. G. Danly, P. Woskoboinikow, W.J. Mulligan, R.J. Temkin, Int. J. Electron., **57**, (1984), p. 851.

(25) K.E. Kreischer and R.J. Temkin, Phys. Rev. Lett., **59**, (1987), p. 547.

(26) J.Y. Ma and L.C. Robinson, Optica Acta., **30**, (1983), p. 1685.

(27) M.N. Afsar, IEEE Trans. on Microwave Theory and Tech., **MTT-32**, (1984) p. 1598.

(28) R.E. Collin, in "Foundations of Microwave Engineering" (McGraw-Hill Book Company, New York, 1966) p. 110.

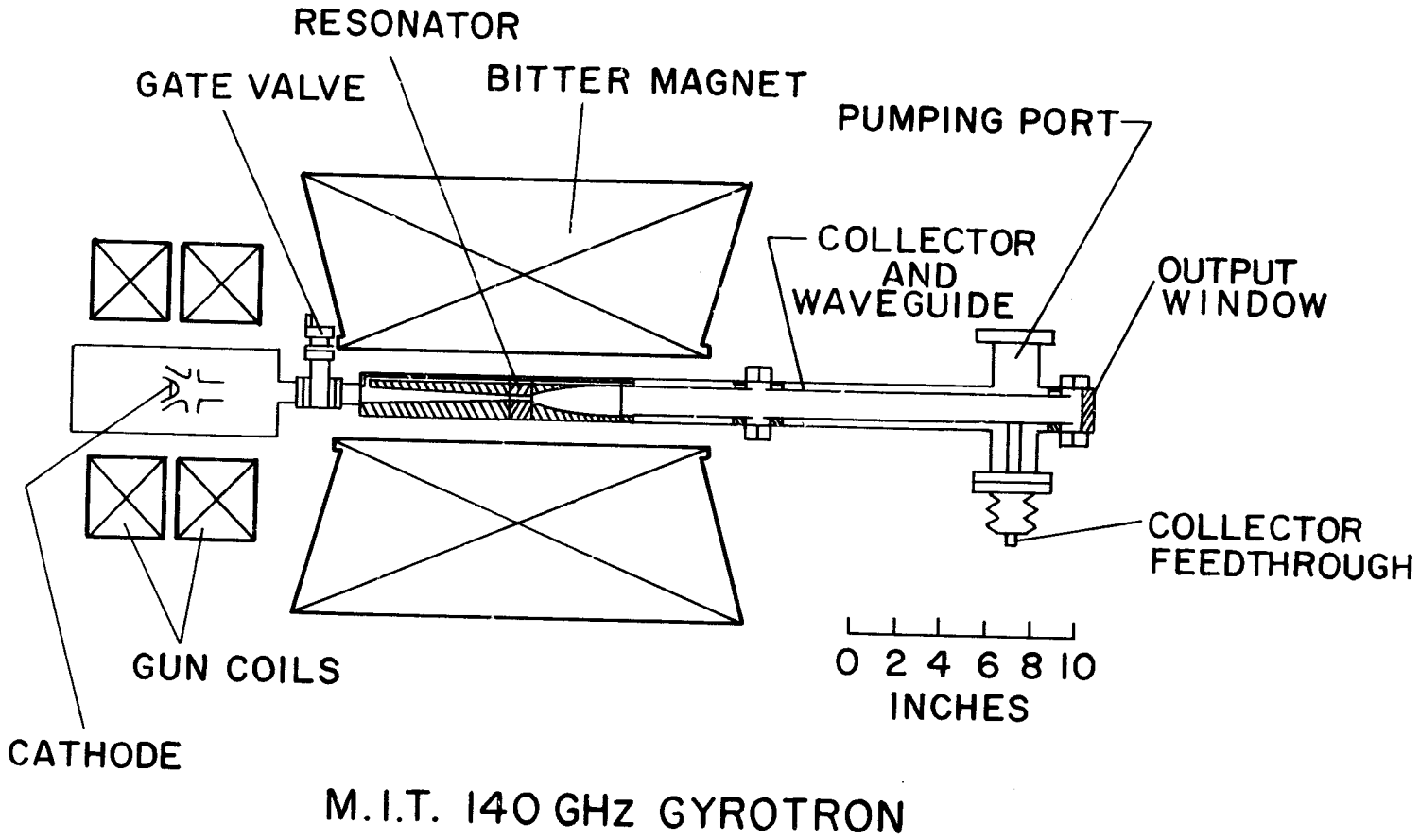

Figure 1 Schematic Diagram of the Second Harmonic Gyrotron

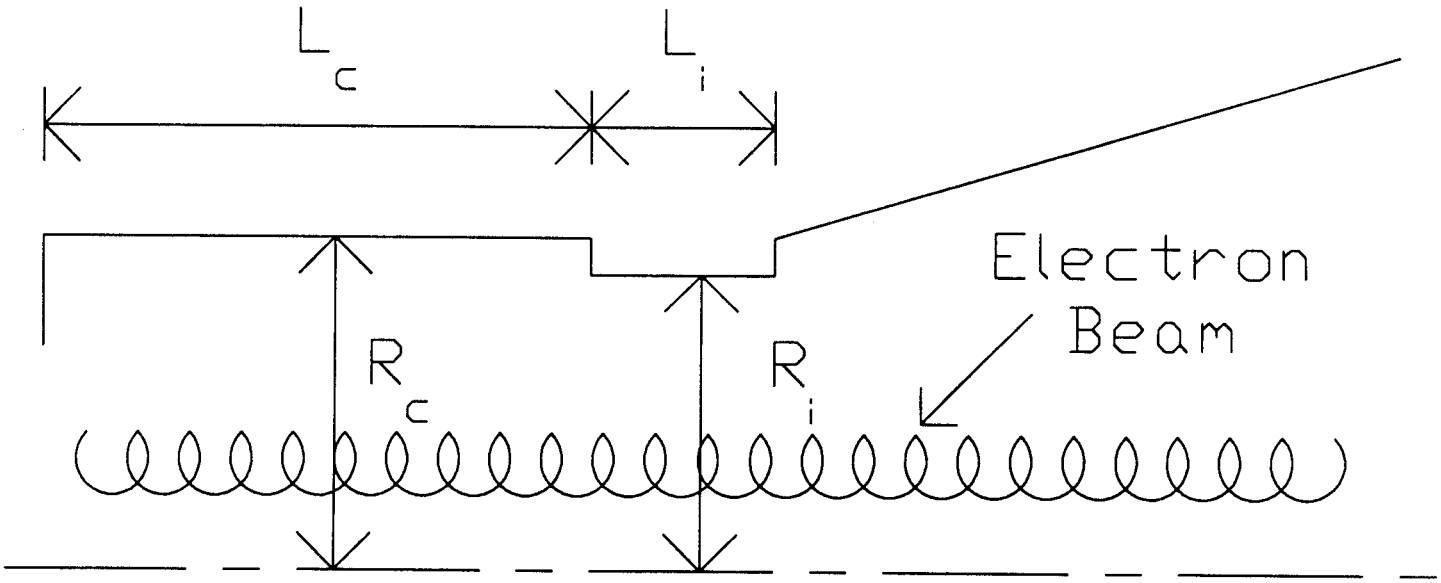

Figure 2 Schematic of a simplified resonator and iris system

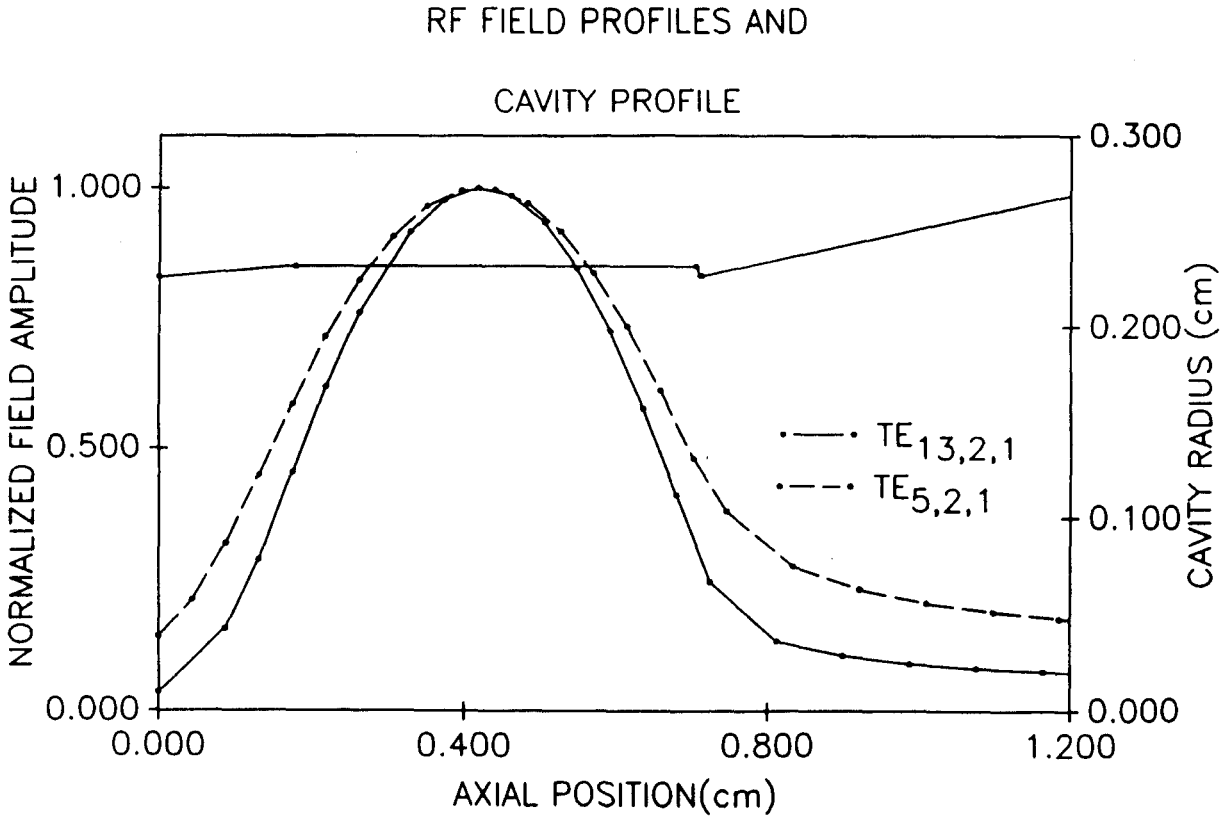

Figure 3 RF field profiles for the fundamental $TE_{5,2,1}$ mode and the second harmonic $TE_{13,2,1}$ mode as a function of axial position for the high Q output iris cavity.

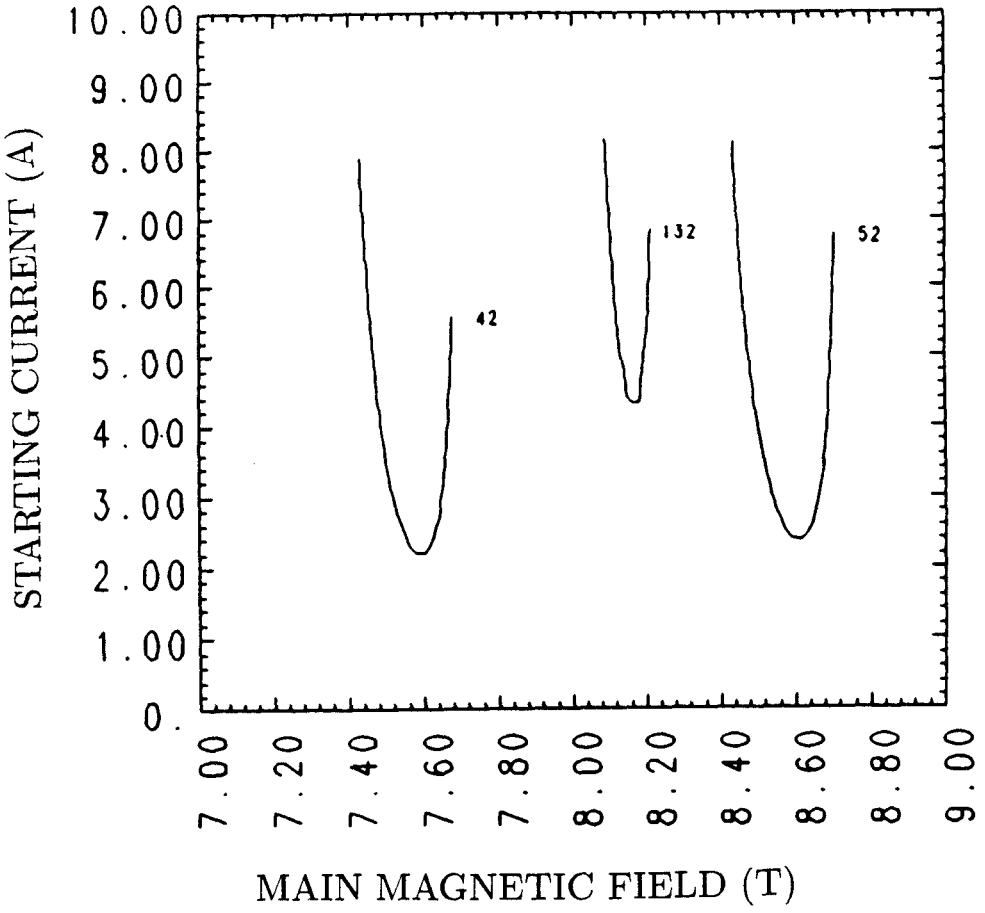

Figure 4a Starting currents for the second harmonic mode and the two strongest fundamental modes. (No iris case with no beam spread.)

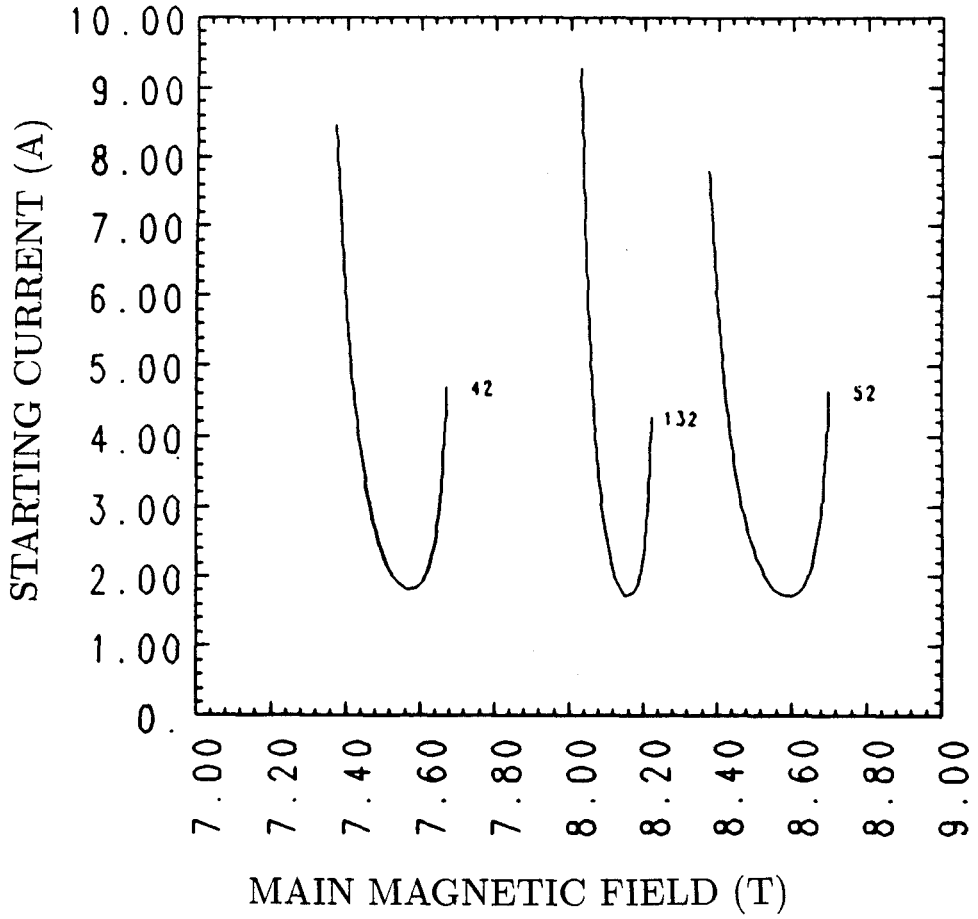

Figure 4b Starting currents for the second harmonic mode and the two strongest fundamental modes. (Iris case with no beam spread.

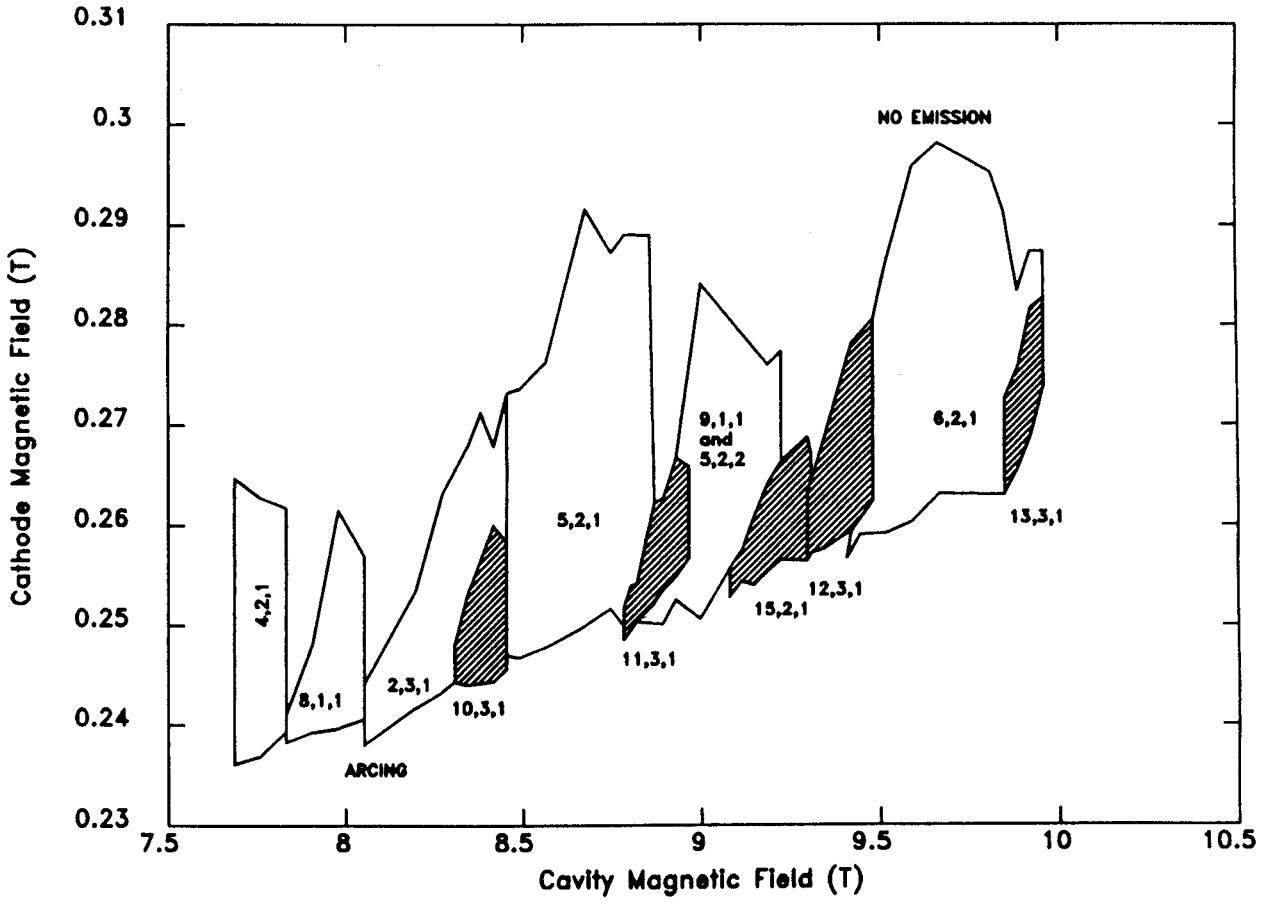

Figure 5 Mode map for the high Q iris cavity with a 14 T magnet at 3 A and 73 kV with quartz window.

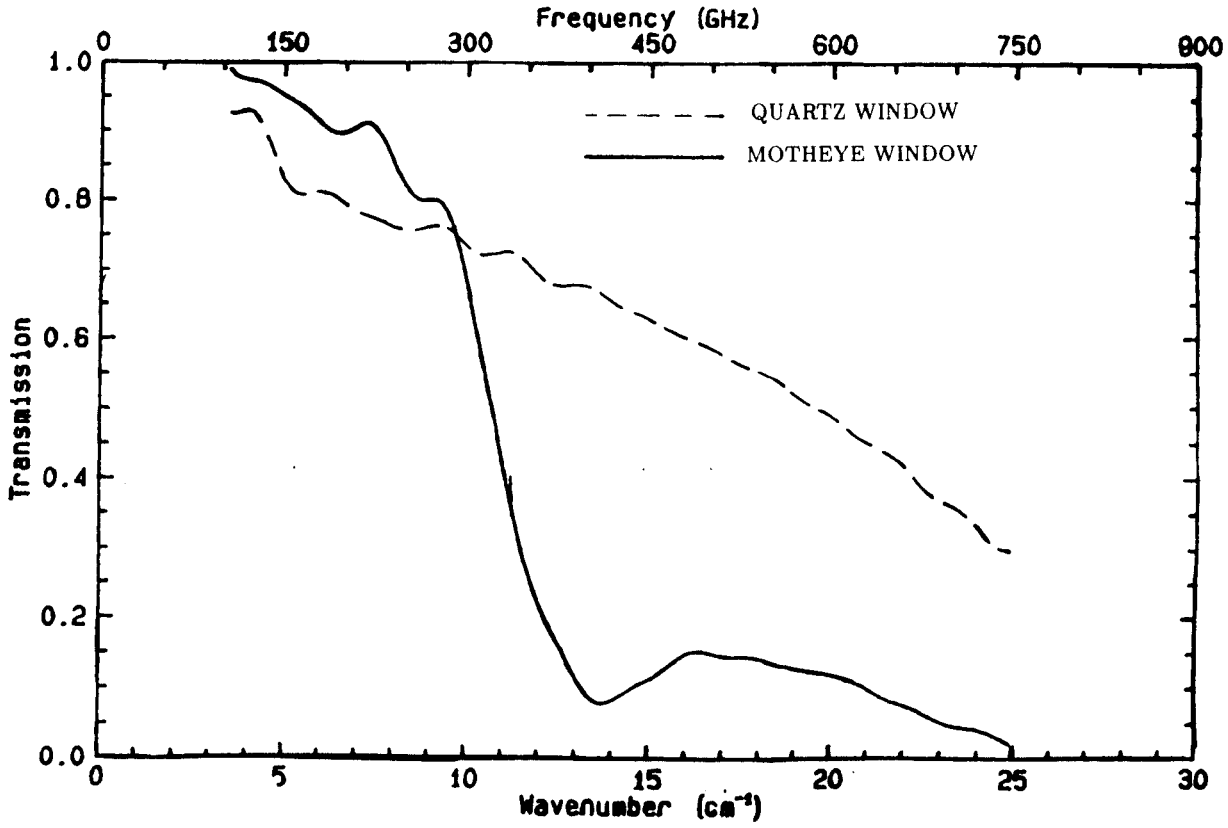

Figure 6 Transmission curve as a function of frequency for the motheye window (very reflective at high frequency)

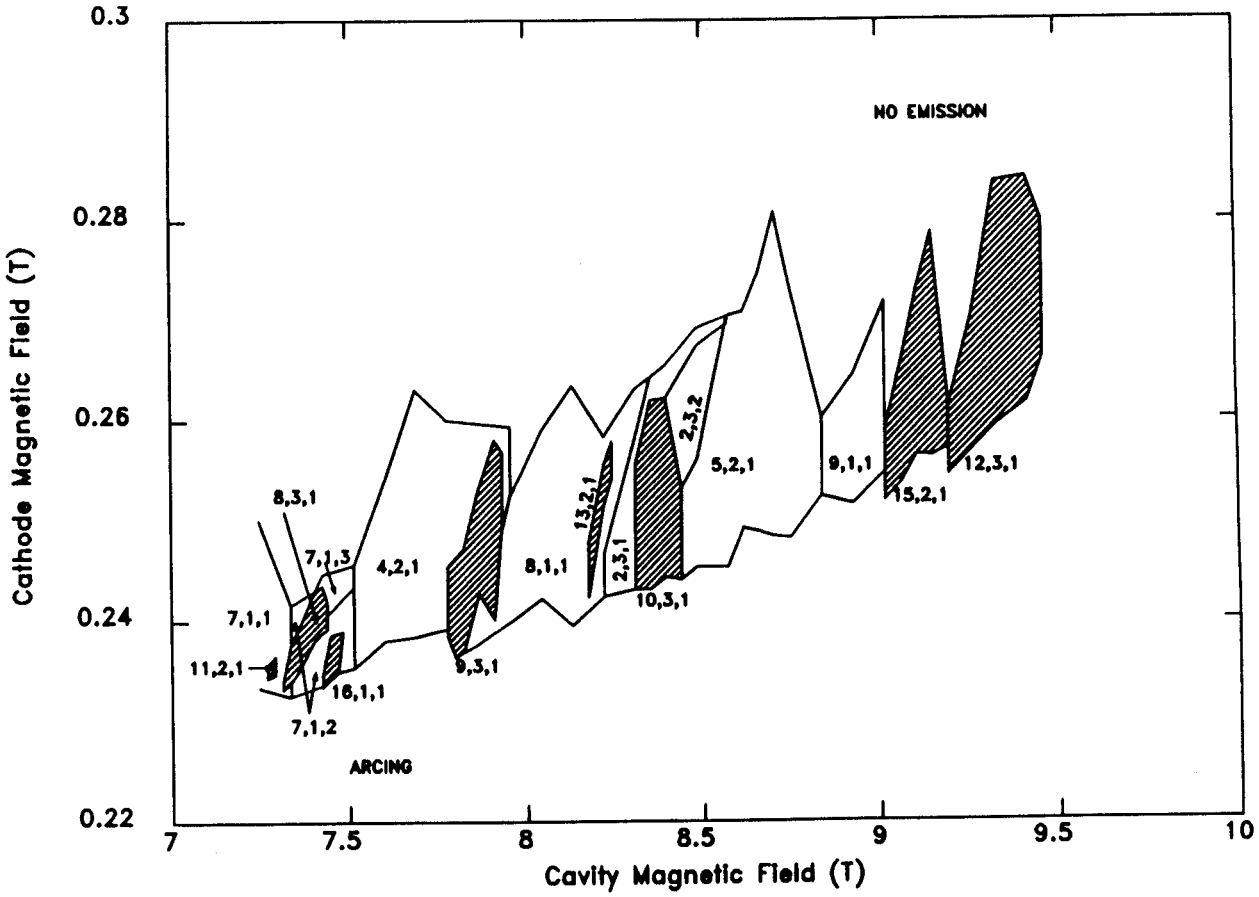

Figure 7 Modemap for the output iris cavity with the motheye window at $I_B = 3\ A$ and $V_c = 73\ kV$.

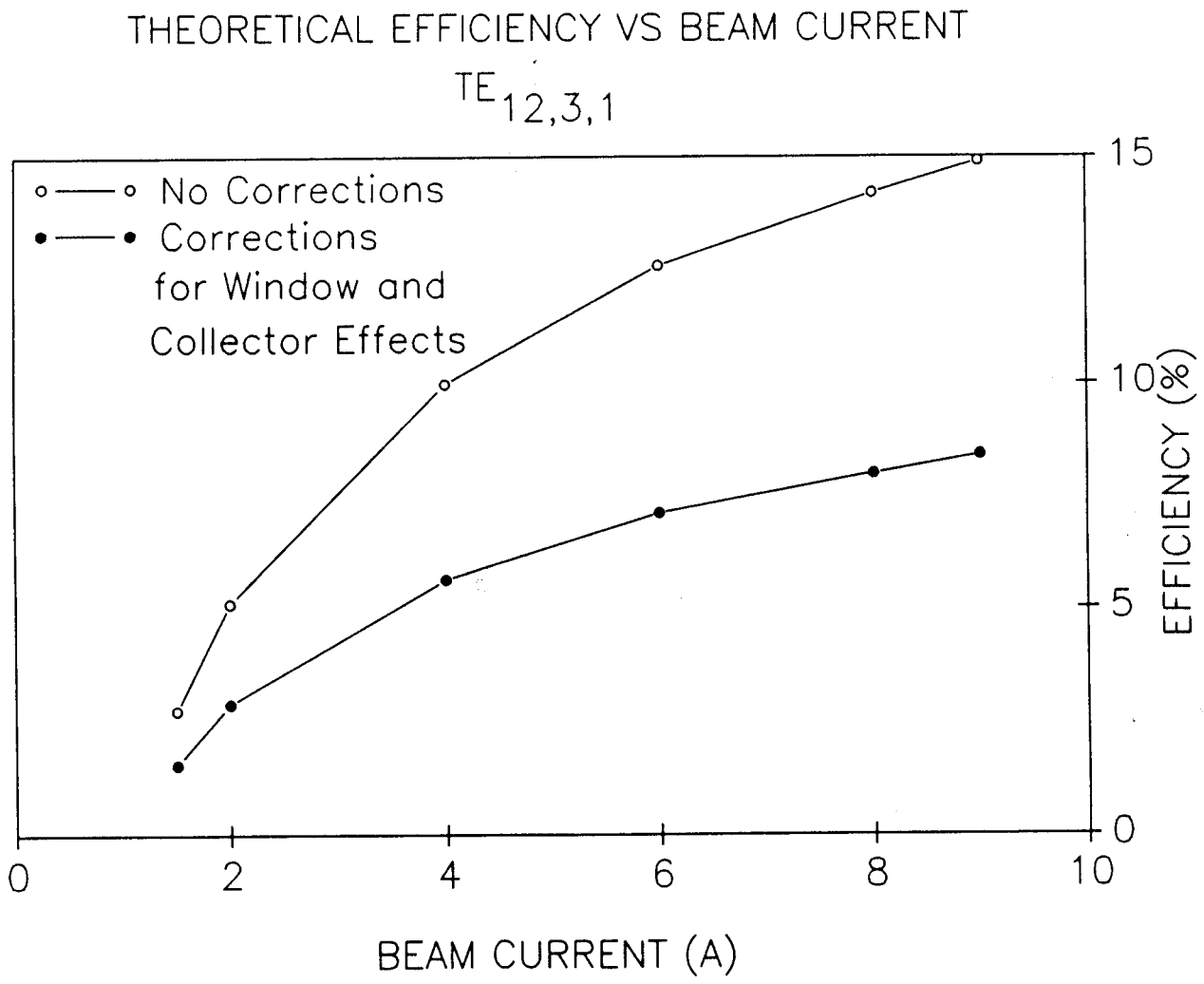

Figure 8a Theoretical efficiency as a function of beam current for the second harmonic $TE_{12,3,1}$ mode at $V_c = 73\ kV$, $\alpha = 1.5$

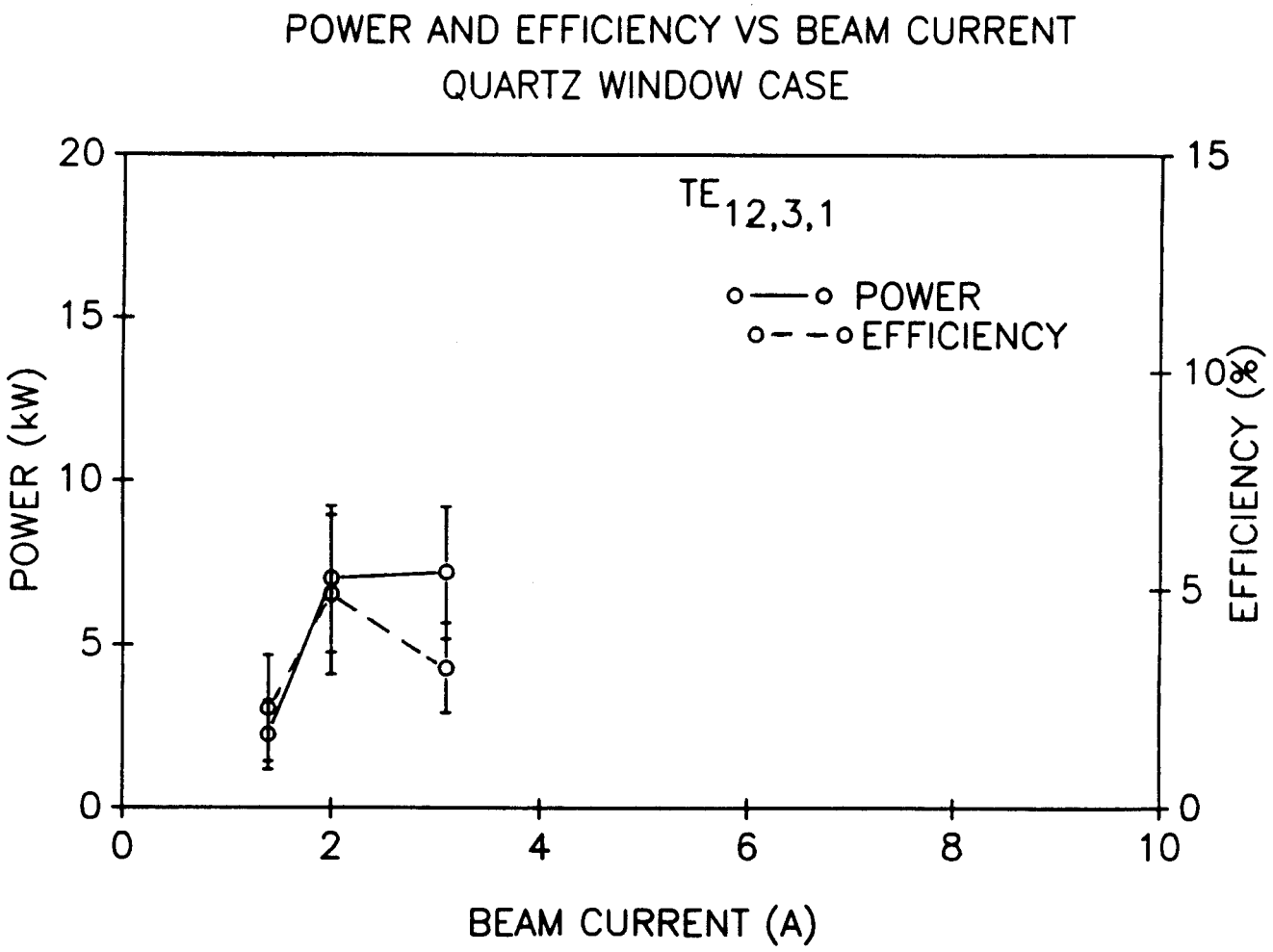

Figure 8b Experimentally measured power and efficiency as functions of beam current at $V_c = 73\ kV$ for the $TE_{12,3,1}$ mode with a quartz window.

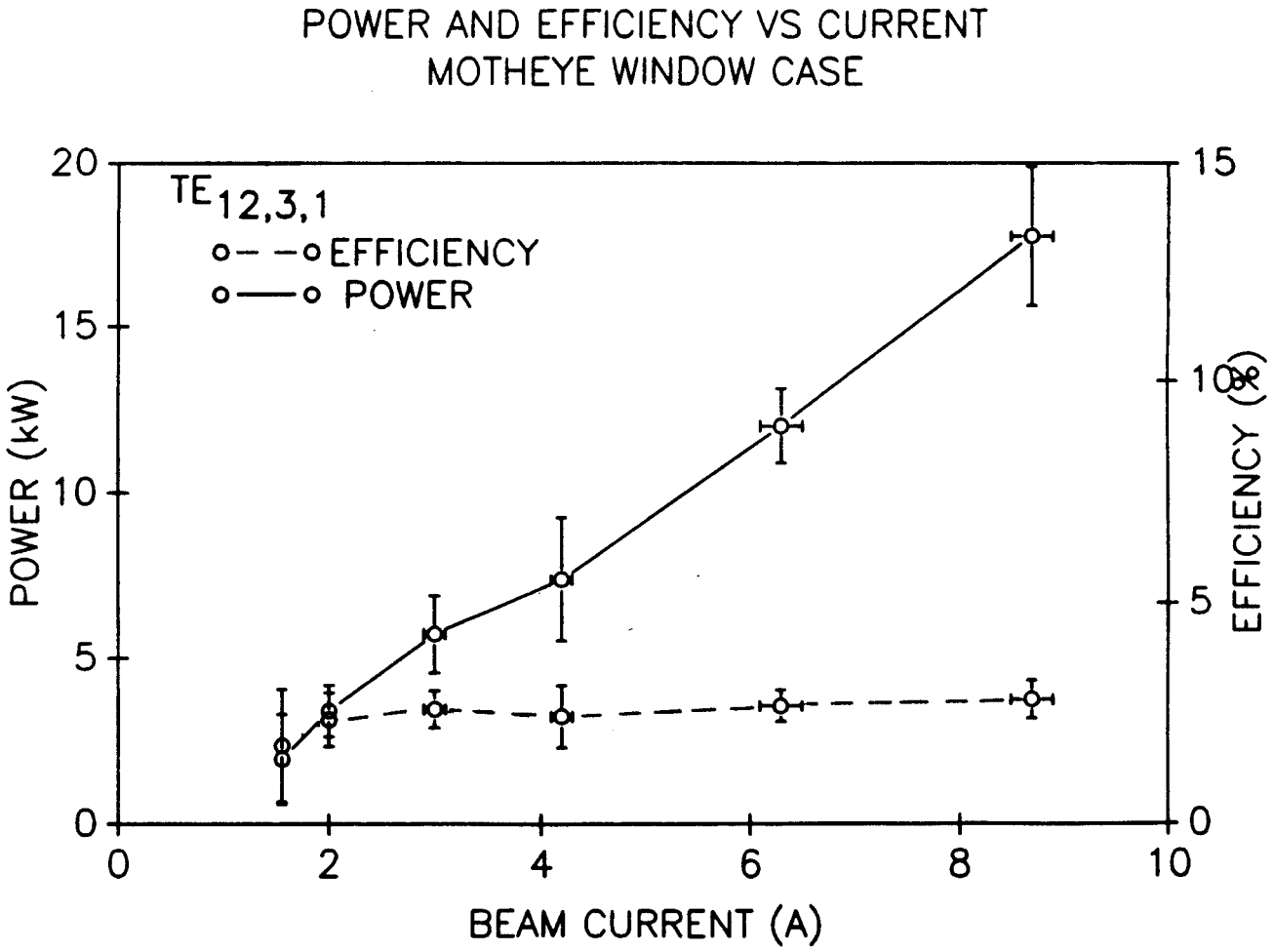

Figure 8c Experimentally measured power and efficiency as functions of beam current at $V_c = 73\ kV$ for the $TE_{12,3,1}$ mode with a motheye window.

TABLE 1

OUTPUT IRIS CAVITY DESIGN PARAMETERS FOR THE HIGH Q RESONATOR

Second Harmonic

Frequency = 410 GHz	Beam Current = 9 Amps
Power = 101 kW	η_T = 17.3 %
Magnetic Field = 8.3 Tesla	Magnetic Field at the Gun = 0.221 Tesla
Cathode Voltage = 65 kV	

TABLE 2

Second harmonic emission observed in the
high Q output iris cavity with the quartz window

Frequency (GHz)	Magnetic Field (T)	Power (kW)	Efficiency (%)	TE Mode
301.6	6.1	4	1.3	$TE_{3,4,1}$
329.6	6.7	5	2.6	$TE_{14,1,1}$
339.3	6.9	4	2.9	$TE_{10,2,1}$
363.3	7.4	7	2.4	$TE_{11,2,1}$
366.9	7.4	4	1.7	$TE_{8,3,1}$
372.6	7.6	4	1.7	$TE_{16,1,1}$
417.1	8.4	15	6.0	$TE_{10,3,1}$
442.8	8.8	14	5.73	$TE_{11,3,1}$
457.1	9.1	≥ 1		$TE_{15,2,1}$
467.2	9.4	9.7	4.8	$TE_{12,3,1}$
492.0	9.9	1.5	0.6	$TE_{13,3,1}$
503.3	10.1	≥ 1		$TE_{17,2,1}$

TABLE 3

Second harmonic emission observed in the
high Q output iris cavity with the motheye window

Frequency (GHz)	Magnetic Field (T)	Power (kW)	Efficiency (%)	TE Mode
339.8	6.8	≥ 1		$TE_{10,2,1}$
363.3	7.4	≥ 1		$TE_{11,2,1}$
366.9	7.4	≥ 1		$TE_{8,3,1}$
372.6	7.6	≥ 1		$TE_{16,1,1}$
392.5	7.8	4	1.8	$TE_{9,3,1}$
410.6	8.2	1	0.7	$TE_{13,2,1}$
417.1	8.4	9	4.1	$TE_{10,3,1}$
457.1	9.1	7	2.1	$TE_{15,2,1}$
467.2	9.3	22	3.4	$TE_{12,3,1}$
492.0	9.8	≥ 1		$TE_{13,3,1}$
503.3	10.2	10	5.33	$TE_{17,2,1}$